

New effective luminescent materials based on the Sm-doped borate glasses

Bohdan V. Padlyak^{1,2*}, Ihor I. Kindrat¹, Radosław Lisiecki³, Volodymyr T. Adamiv², Ihor M. Teslyuk²

¹Division of Spectroscopy of Functional Materials, Institute of Physics, University of Zielona Góra, 4a Szafrana str., 65-516 Zielona Góra, Poland

²Department of Optical Materials, Vlokh Institute of Physical Optics, 23 Dragomanov str., 79-005 Lviv, Ukraine

³Department of Spectroscopy of Laser Materials, Division of Optical Spectroscopy, Institute of Low Temperature and Structure Research Polish Academy of Sciences, 2 Okólna str, 50-422 Wrocław, Poland

*Corresponding author, Tel: (+48) 68 328 2904; E-mail: B.Padlyak@if.uz.zgora.pl

Received: 03 October 2016, Revised: 13 November 2016 and Accepted: 20 December 2016

DOI: 10.5185/amlett.2017.1436
www.vbripress.com/aml

Abstract

The spectroscopic and radiative properties of the Sm-doped borate glasses with $\text{Li}_2\text{B}_4\text{O}_7$, LiKB_4O_7 , CaB_4O_7 , and LiCaBO_3 basic compositions as new luminescent materials have been investigated and analysed. The borate glasses of high chemical purity and optical quality, doped with Sm_2O_3 in amounts of 0.5 and 1.0 mol. % were obtained from corresponding polycrystalline compounds in the air atmosphere using standard glass synthesis technology. The spectroscopic properties of obtained Sm-doped glasses were studied using electron paramagnetic resonance (EPR), optical absorption, photoluminescence, and decay kinetics techniques. The Judd–Ofelt theory had been used for analysis of the optical absorption spectra and calculation of the phenomenological intensity parameters (Ω_2 , Ω_4 , Ω_6). Radiative properties such as transition probabilities (A_{rad}), branching ratios (β_{exp} and β_{rad}), stimulated emission cross-sections (σ_e), and radiative lifetimes (τ_{rad}) were estimated for $^4\text{G}_{5/2} \rightarrow ^6\text{H}_j$ ($J = 5/2, 7/2, 9/2, \text{ and } 11/2$) emission transitions of the Sm^{3+} ions in the $\text{Li}_2\text{B}_4\text{O}_7:\text{Sm}$, $\text{CaB}_4\text{O}_7:\text{Sm}$, and $\text{LiCaBO}_3:\text{Sm}$ glasses containing 1.0 mol. % Sm_2O_3 . The luminescence kinetics of Sm^{3+} centres in the investigated glasses are characterised by a single exponent decay with typical lifetimes, which depend on the basic glass composition and Sm impurity concentration. Experimental lifetimes (τ_{exp}) have been compared with those calculated (τ_{rad}) and quantum efficiencies (η) of the Sm^{3+} emission transitions were estimated. The calculated high quantum efficiencies ($\sim 80\%$) and measured high quantum yields of luminescence ($\sim 14 - 21\%$) clearly show that the investigated glasses belong to very promising materials for luminescent and laser applications. Copyright © 2017 VBRI Press.

Keywords: Borate glasses, Sm^{3+} ions, optical absorption, luminescence spectra, Judd–Ofelt analysis, luminescence kinetics, radiative properties.

Introduction

In the last decade, the investigation of borate glasses presents significant practical interest due to their attractive physical, optical, and luminescence properties [1–8]. This interest is caused with simple and inexpensive producing technology of the borate glasses in comparison with their crystalline analogues as well as their good thermal stability, high transparency in wide spectral range, and possibility of doping by rare earth (RE) and transition elements in wide concentration range.

Attractive optical and spectroscopic properties and high quantum yield of luminescence of the RE doped materials allow their wide applications for laser technique, energy transformation, telecommunication, display devices, sensors, etc. [9,10]. In particular, the undoped and doped borate compounds represent very promising materials for nonlinear optics and laser

techniques [5,11–15], scintillates and thermoluminescence dosimeters [16–18], detectors and transformers of ionising radiation [19,20], and many other applications [21–22]. This especially concerns to the single crystals of lithium tetraborate ($\text{Li}_2\text{B}_4\text{O}_7$), which are characterised by high transparency in very wide spectral region (from vacuum ultraviolet (UV) to middle infrared (IR)) [23] and extremely high stability to the ionising radiation [24,25]. Thus, perspectives of wide applications of the RE doped borate glasses and crystals stimulate the synthesis of new boron-containing optical materials and intensive study of their luminescent and spectroscopic properties and parameters.

The intensity of optical absorption bands corresponding to the RE ions in different hosts can be calculated with usage the Judd–Ofelt (J–O) theory [26,27]. This theory defines a set of three phenomenological intensity parameters (Ω_2 , Ω_4 , Ω_6),

which are very sensitive to the local structure of the RE ions in the crystal lattice or glass network. The intensity parameters (Ω_2 , Ω_4 , Ω_6) can be used for calculations of the following parameters of various emission lines for RE impurity ions: probabilities of the radiative transitions, radiative lifetimes of the excited states, branching ratios, and stimulated emission cross-sections. All these parameters are required in order to evaluate the obtained ion-host configuration and the luminescence efficiency of the specific electronic transitions at developing novel materials for lasers and other optical devices with desired optimal luminescent characteristics.

Crystals and glasses, activated with Sm^{3+} ions are well-known as efficient luminescent materials, which characterised by high quantum yield at room temperature as well as good thermal and chemical stability in the air atmosphere [9,28]. The Sm^{3+} ions in oxide crystals and glasses reveal characteristic intense green, orange, and red emission bands, which correspond to the ${}^4\text{G}_{5/2} \rightarrow {}^6\text{H}_{5/2}$, ${}^4\text{G}_{5/2} \rightarrow {}^6\text{H}_{7/2}$, and ${}^4\text{G}_{5/2} \rightarrow {}^6\text{H}_{9/2}$ emission transitions, respectively and can be used in modern light sources, display panels, UV-sensors, and visible lasers [29–32]. The quantum efficiency of luminescence of the Sm^{3+} centres is relatively high, because large energy gap between the ${}^4\text{G}_{5/2}$ metastable state and the next lower level leads to low rate of multiphonon relaxation for Sm^{3+} [33].

At present time, spectroscopic and luminescence properties of the Sm^{3+} ions already have been investigated in the borate glasses with various compositions [29–44]. It should be noted that the influence of glass host and Sm concentration are essential for obtaining luminescent properties and parameters suitable for practical applications. The variation of local structure of the Sm^{3+} ions in alkali or alkaline earth borate glasses [4] allows investigating the relationship between the basic glass composition, Sm impurity concentration, and efficiency of their luminescence. In this aspect, special scientific and practical interest represents a series of Sm-doped glasses with $\text{Li}_2\text{B}_4\text{O}_7$, KLiB_4O_7 , CaB_4O_7 , and LiCaBO_3 basic compositions, which correspond to their crystalline analogues [4–8].

This article presents spectroscopic and luminescence properties for a series of Sm-doped borate glasses with $\text{Li}_2\text{B}_4\text{O}_7$, LiKB_4O_7 , CaB_4O_7 , and LiCaBO_3 compositions, which were investigated using conventional spectroscopy methods, including electron paramagnetic resonance (EPR), optical absorption, photoluminescence, and decay kinetics. The J–O analysis of Sm^{3+} ions in the borate glasses has been carried out for predicting radiative properties and parameters such as probabilities of emission transitions, lifetimes, branching ratios, and emission cross-sections. Present article especially is focused on the evaluation of luminescent materials based on the investigated borate glasses activated with Sm^{3+} ions, which exhibit superior optical and radiative properties and can be used for effective UV – visible converters of sun radiation in the Si-based solar cells.

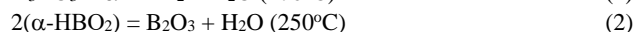
Experimental

Technology of the Sm-doped borate glasses

The Sm-doped borate glasses with $(\text{Li}_2\text{O} - 2\text{B}_2\text{O}_3)$, $(0.5\text{Li}_2\text{O} - 0.5\text{K}_2\text{O} - 2\text{B}_2\text{O}_3)$, $(\text{CaO} - 2\text{B}_2\text{O}_3)$, and $(0.5\text{Li}_2\text{O} - \text{CaO} - 0.5\text{B}_2\text{O}_3)$ basic compositions were obtained in air atmosphere from corresponding polycrystalline compounds of the $\text{Li}_2\text{B}_4\text{O}_7$, LiKB_4O_7 , CaB_4O_7 , and LiCaBO_3 compositions, respectively using standard glass synthesis and technological conditions, which have been described in [4].

Carbonates (Li_2CO_3 , K_2CO_3 , and CaCO_3) and boric acid (H_3BO_3) of high chemical purity (99.999 %, Aldrich) have been used for solid-state synthesis of the $\text{Li}_2\text{B}_4\text{O}_7$, LiKB_4O_7 , CaB_4O_7 , and LiCaBO_3 polycrystalline compounds. The samarium dopant has been added to the raw materials as Sm_2O_3 oxide of chemical purity (99.99 %) in amounts of 0.5 and 1.0 mol. %.

Solid-state synthesis of the polycrystalline borate compounds has been done using multi-step heating chemical reactions [4], which can be described by the following equations:



Large bulk samples of the Sm-doped $\text{Li}_2\text{B}_4\text{O}_7$, LiKB_4O_7 , CaB_4O_7 , and LiCaBO_3 glasses have been obtained by fast cooling of the corresponding melts. These melts were heated more than 100 K above the melting points ($T_{\text{melt}} = 917^\circ\text{C}$ (1190 K), 807°C (1080 K), 980°C (1253 K), and 777°C (1050 K) for $\text{Li}_2\text{B}_4\text{O}_7$, LiKB_4O_7 , CaB_4O_7 , and LiCaBO_3 compounds, respectively) for blocking of the undesirable crystallisation process [4]. The glass samples for optical measurements were cut and polished to the approximate size of $5 \times 4 \times 2 \text{ mm}^3$.

Experimental equipment and short characterisation of the investigated borate glasses

The paramagnetic impurities in the investigated Sm-doped borate glasses were detected in the $4 \div 50 \text{ K}$ temperature range with usage commercial X-band EPR spectrometer BRUKER (model ELEXSYS E-500) completed with helium-flow cryostat (OXFORD Instruments) as well as modernised X-band spectrometers RADIOPAN (models SE/X-2013 and SE/X-2544) that working at room temperature (RT).

The optical absorption spectra were registered using a Cary 5000 (Agilent Technologies), Varian (model 5E UV-VIS-NIR), and SHIMADZU (model 2450 UV-VIS) commercial spectrophotometers. The photoluminescence spectra (emission and excitation) as well as luminescence decay curves were recorded in the UV – visible spectral ranges at RT with usage a HORIBA (model FluoroMax-4) spectrofluorimeter. The luminescence quantum yields were measured using a Hamamatsu Absolute PL quantum yield measurement system (model C9920-02G).

The X-ray diffraction (XRD) investigations were carried out with usage a computer-controlled X-ray

diffractometer of DRON-3 type and monochromatic Cu K_{α} line ($\lambda = 1.544 \text{ \AA}$). The X-ray diffractograms have been recorded in the $10^{\circ} < 2\theta < 110^{\circ}$ range with step scanning of 0.015° and rate of $2^{\circ}/\text{min}$. Typical XRD patterns for $\text{CaB}_4\text{O}_7:\text{Sm}$, $\text{LiKB}_4\text{O}_7:\text{Sm}$, and $\text{LiCaBO}_3:\text{Sm}$ glasses containing 1.0 mol. % Sm_2O_3 are presented in **Fig. 1a**. The absence of discrete sharp peaks in the obtained XRD patterns confirms disorder glass structure of the investigated materials. The average interatomic distances in the investigated Sm-doped borate glasses were derived from pair correlation functions, which were obtained by Fourier transformation of XRD patterns and published in [8].

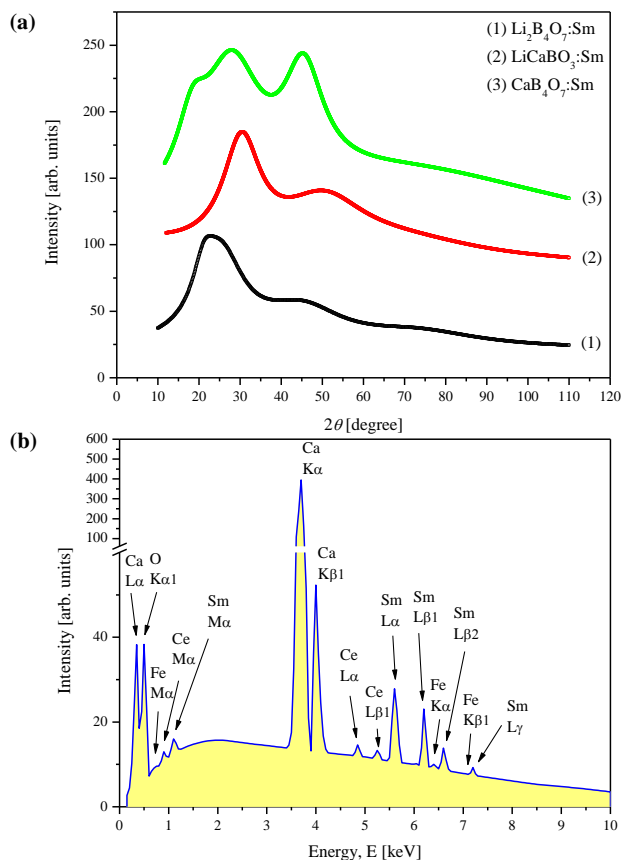


Fig. 1. (a) The XRD patterns of borate glasses with $\text{Li}_2\text{B}_4\text{O}_7:\text{Sm}$, $\text{LiCaBO}_3:\text{Sm}$, and $\text{CaB}_4\text{O}_7:\text{Sm}$ compositions containing 1.0 mol. % Sm_2O_3 ; (b) The EDS spectrum of the $\text{CaB}_4\text{O}_7:\text{Sm}$ glass containing 1.0 mol. % Sm_2O_3 .

The un-doped $\text{Li}_2\text{B}_4\text{O}_7$ glasses are transparent in the $281 \div 2760 \text{ nm}$ spectral range [20], whereas the un-doped single crystals with same composition are characterised by high transparency in the spectral region of $167 \div 3200 \text{ nm}$ [23]. Our un-doped glasses with $\text{Li}_2\text{B}_4\text{O}_7$, LiKB_4O_7 , CaB_4O_7 , and LiCaBO_3 compositions are transparent in the spectral range of $300 \div 2500 \text{ nm}$. The Sm-doped borate glasses are almost uncoloured and characterised by a high optical quality. The Sm concentrations have been proved by method of X-ray energy dispersive spectroscopy (EDS) using scanning electron microscope of the REMMA-102-02 type (Selmi, Ukraine). The EDS of obtained glasses confirms presence of the Sm_2O_3 in

amounts 0.5 and 1.0 mol. % for corresponding samples. Hence, the coefficient of incorporation of the Sm impurity into the network of investigated glass is close to unity. Obtained EDS spectrum for $\text{CaB}_4\text{O}_7:\text{Sm}$ ($\text{Sm}_2\text{O}_3 - 1.0 \text{ mol. \%}$) glass sample is presented in **Fig. 1b**. One can notice that besides Sm, the Ce non-controlled impurity was detected by EDS in amounts $0.05 \div 0.07$ and $0.10 \div 0.15 \text{ mol. \%}$ in the glass samples containing 0.5 and 1.0 mol. % Sm_2O_3 , respectively. Thus, our Sm-doped borate glasses are self-co-doped with cerium.

For $\text{Li}_2\text{B}_4\text{O}_7:\text{Sm}$, $\text{LiCaBO}_3:\text{Sm}$, and $\text{CaB}_4\text{O}_7:\text{Sm}$ glasses containing 1.0 mol. % Sm_2O_3 the refractive indices, measured at $\lambda = 632.8 \text{ nm}$ are equal 1.524, 1.528, and 1.544, respectively. The densities of investigated glasses, measured by the Archimedes method, are equal 2.22, 2.47, and 2.48 g/cm^3 , respectively for $\text{Li}_2\text{B}_4\text{O}_7:\text{Sm}$, $\text{LiCaBO}_3:\text{Sm}$, and $\text{CaB}_4\text{O}_7:\text{Sm}$ glasses containing 1.0 mol. % Sm_2O_3 .

Results and discussion

The results of spectroscopic study of the Sm-doped lithium tetraborate ($\text{Li}_2\text{B}_4\text{O}_7:\text{Sm}$) glasses for the first time have been presented in [45]. Previous results of the EPR and optical spectroscopy for $\text{Li}_2\text{B}_4\text{O}_7:\text{Sm}$, $\text{LiKB}_4\text{O}_7:\text{Sm}$, $\text{CaB}_4\text{O}_7:\text{Sm}$, and $\text{LiCaBO}_3:\text{Sm}$ glasses were reported in [46] and published in [8,47]. In this article are summarised our results of spectroscopic investigations of the Sm-doped borate glasses as a new perspective luminescent materials, especially for UV – visible converters of the sun radiation in the Si-based solar cells.

The EPR spectroscopy of Sm-doped borate glasses

The Sm impurity can be incorporated into the structure of oxide compounds as paramagnetic Kramers Sm^{3+} ($4f^5$, $^6\text{H}_{5/2}$) ions or non-Kramers Sm^{2+} ($4f^6$, $^7\text{F}_0$) ions. The Sm ions can be identified due to their characteristic EPR, optical absorption, and luminescence spectra. Up to now the EPR spectra of Sm^{3+} and other rare-earth non-S-state Kramers ions in glasses and other disordered solids are studied insufficiently. The X-band EPR spectra of the non-S-state Kramers rare-earth ions (Ce^{3+} , Nd^{3+} , Dy^{3+} , Er^{3+} , Yb^{3+}) in zeolites and glasses according to [48] consist of extremely broad asymmetric signals, which can be observed at liquid helium temperatures only. The referenced data on EPR spectroscopy of the Sm^{3+} ions in glasses and other disordered solids are absent at present time [48].

The EPR spectra, registered in all our un-doped borate glasses at RT are almost identical and contain intense line with effective g -factor, $g_{\text{eff}} \cong 4.26$ and weak line with $g_{\text{eff}} \cong 2.00$ (**Fig. 2a**, spectrum 1). The EPR line with $g_{\text{eff}} \cong 4.26$ that denoted as $\text{Fe}^{3+}(1)$ in **Fig. 2**, is characteristic for glasses and belongs to single (isolated) Fe^{3+} ($3d^5$, $^6\text{S}_{5/2}$) ions of the iron non-controlled impurity localised in the octahedral and/or tetrahedral sites with a strong rhombic distortion [49–53]. The weak EPR line with $g_{\text{eff}} \cong 2.00$ that denoted as $\text{Fe}^{3+}(2)$ in **Fig. 2**, belongs to the Fe^{3+} isolated (single) centres, located in the glass network sites with nearly cubic local symmetry [49,51].

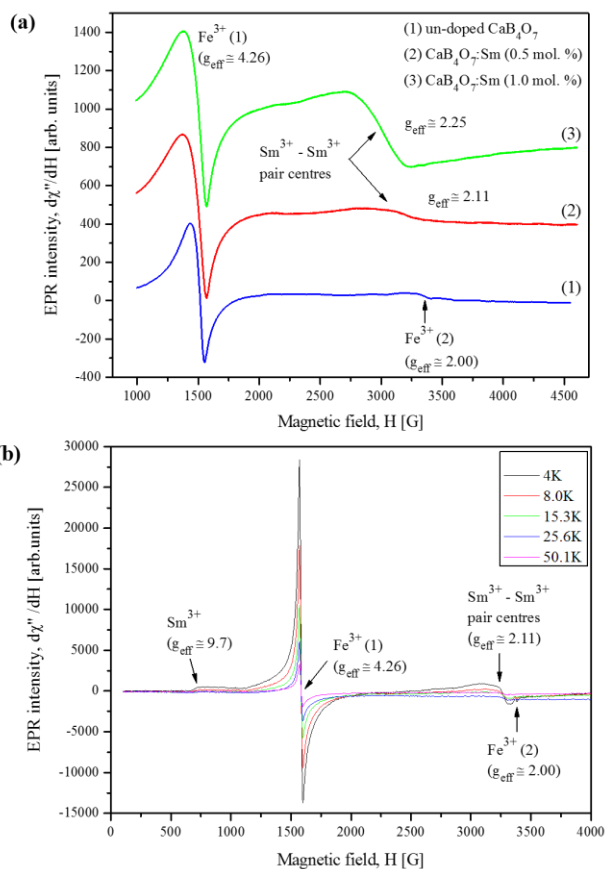


Fig. 2. (a) The X-band ($\nu \approx 9.433$ GHz) EPR spectra of un-doped CaB_4O_7 glass and $\text{CaB}_4\text{O}_7:\text{Sm}$ glasses with 0.5 and 1.0 mol. % Sm_2O_3 , registered at $T = 300$ K; (b) The X-band ($\nu \approx 9.457$ GHz) EPR spectra of the $\text{Li}_2\text{B}_4\text{O}_7:\text{Sm}$ glass with 0.5 mol. % Sm_2O_3 , registered in the temperature range $4 \div 50$ K.

Besides the Fe^{3+} EPR lines with $g_{\text{eff}} \approx 4.26$ and $g_{\text{eff}} \approx 2.00$ in the EPR spectra of all examined by us Sm-doped borate glasses at RT have been registered new broad signals with $g_{\text{eff}} \approx 2.11$ and $g_{\text{eff}} \approx 2.25$ for samples containing 0.5 and 1.0 mol. % Sm_2O_3 , respectively (see **Fig. 2a**, spectra 2 and 3). Increasing of the Sm_2O_3 content in the investigated glasses leads to the following effects for this new broad EPR signal: increasing of integral intensity, lowering of resonance field, and some decreasing of linewidth (**Fig. 2a**, spectra 2 and 3). Based on the observed effects one can assumed that this new EPR signal, observed in all Sm-doped glasses at RT, belongs to the $\text{Sm}^{3+} - \text{Sm}^{3+}$ pair centres, which are coupled by magnetic dipolar and exchange interactions.

The additional broad EPR signal was observed in all investigated Sm-doped borate glasses at low temperatures. The new asymmetric EPR signal with $g_{\text{eff}} \approx 9.7$ that has been observed in the $4.2 \div 20$ K temperature range in $\text{Li}_2\text{B}_4\text{O}_7:\text{Sm}$ glass containing 0.5 mol. % Sm_2O_3 is presented in **Fig. 2b**. This EPR signal is associated with the single Sm^{3+} centres. The EPR signal of single Sm^{3+} centres disappear about $T = 20$ K (see **Fig. 2b**) due to shortening of their spin-lattice relaxation time. Thus, EPR spectroscopy at room and liquid helium temperatures demonstrates presence of the Sm^{3+} single and $\text{Sm}^{3+} -$

Sm^{3+} pair centres in all investigated Sm-doped borate glasses.

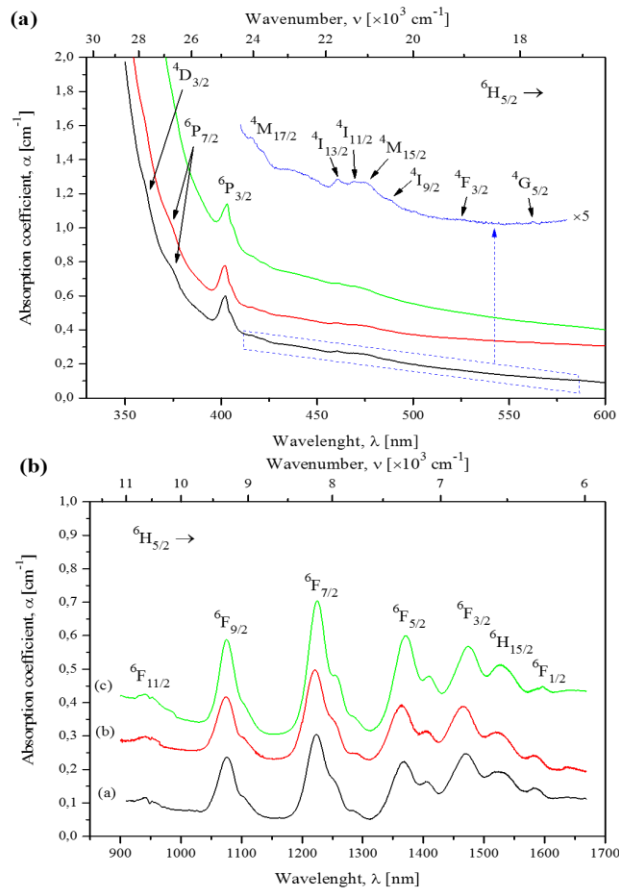


Fig. 3. The optical absorption spectra of glasses with $\text{Li}_2\text{B}_4\text{O}_7:\text{Sm}$ (black curves), $\text{CaB}_4\text{O}_7:\text{Sm}$ (red curves), and $\text{LiCaBO}_3:\text{Sm}$ (green curves) compositions containing 1.0 mol. % Sm_2O_3 , recorded at RT in the visible (a) and infrared (b) regions.

Optical absorption spectra of the Sm-doped borate glasses and J–O analysis for Sm^{3+} centres

Typical absorption spectra, which were registered in the $\text{Li}_2\text{B}_4\text{O}_7:\text{Sm}$, $\text{CaB}_4\text{O}_7:\text{Sm}$, and $\text{LiCaBO}_3:\text{Sm}$ glasses with 1.0 mol. % Sm_2O_3 are presented in **Fig. 3, a** and **b**. The intense broadband absorption about 350 nm (**Fig. 3a**) belongs to the edge of fundamental absorption of the glass host. In accordance with [54,55] all other observed absorption bands, were assigned to following $f - f$ transitions of the Sm^{3+} centres: ${}^6\text{H}_{5/2} \rightarrow {}^4\text{D}_{3/2}$, ${}^6\text{P}_{7/2}$, ${}^6\text{P}_{3/2}$, ${}^4\text{M}_{17/2}$, ${}^4\text{I}_{13/2}$, ${}^4\text{I}_{11/2}$, ${}^4\text{M}_{15/2}$, ${}^4\text{I}_{9/2}$, ${}^4\text{F}_{3/2}$, and ${}^4\text{G}_{5/2}$ (UV – visible region) (see **Fig. 3a**) as well as: ${}^6\text{H}_{5/2} \rightarrow {}^6\text{F}_{11/2}$, ${}^6\text{F}_{9/2}$, ${}^6\text{F}_{7/2}$, ${}^6\text{F}_{5/2}$, ${}^6\text{F}_{3/2}$, ${}^6\text{H}_{15/2}$, and ${}^6\text{F}_{1/2}$ (infrared region) (see **Fig. 3b**). Transitions from ground ${}^6\text{H}_{5/2}$ state to the ${}^6\text{H}$, ${}^6\text{F}$, and ${}^6\text{P}$ levels are spin-allowed. Therefore, all observed IR absorption bands and visible band that corresponds to the ${}^6\text{H}_{5/2} \rightarrow {}^6\text{P}_{3/2}$ transition are most intense. Other observed visible absorption bands are weak, because correspond to the spin-forbidden transitions.

The Sm^{3+} experimental oscillator strengths (f_{exp}) were calculated using measured area under the observed absorption bands and the following relation [56],

$$f_{\text{exp}} = \frac{2303mc^2}{N_A \pi e^2} \int \varepsilon(\nu) d\nu = 4.32 \times 10^{-9} \int \varepsilon(\nu) d\nu \quad (7)$$

where m is the mass of electron, c is the light velocity, N_A is the number of Avogadro, e is the electron charge, $\varepsilon(\nu)$ is the molar absorption coefficient at wavenumber ν . All values in formula (7) are given in the CGS units. The $\varepsilon(\nu)$ was taken from the Beer–Lambert's law:

$$\varepsilon(\nu) = \frac{1}{cl} \log\left(\frac{I_0}{I}\right) \quad (8)$$

where c is the Sm concentration in mol/l, l is the sample thickness or the optical path length that is given in cm and $\log\left(\frac{I_0}{I}\right)$ is the absorbance or optical density that is taken at wavenumber ν . Obtained values of the experimental oscillator strengths for Sm³⁺ optical absorption bands in the Li₂B₄O₇:Sm, CaB₄O₇:Sm, and LiCaBO₃:Sm glasses are presented in **Table 1**.

Calculated (theoretical) values of the oscillator strength (f_{cal}) for an induced transition between the ground (ψ_J) and excited ($\psi'_{J'}$) states is given by the relation:

$$f_{\text{cal}} = f_{ED} + f_{MD} = \frac{8\pi^2 m c \nu}{3h e^2 (2J+1)} \left(\frac{(n^2+2)^2}{9n} S_{ED} + n S_{MD} \right) \quad (9)$$

$$S_{ED} = e^2 \sum_{\lambda=2,4,6} \Omega_{\lambda} \left| \langle \psi_J \| U^{\lambda} \| \psi'_{J'} \rangle \right|^2 \quad (10)$$

$$S_{MD} = \frac{e^2 h^2}{16\pi^2 m^2 c^2} \left| \langle \psi_J \| L + 2S \| \psi'_{J'} \rangle \right|^2 \quad (11)$$

where Ω_{λ} ($\lambda = 2, 4, 6$) are the phenomenological J–O intensity parameters [26,27] and $\|U^{\lambda}\|^2$ are squared reduced matrix elements for the $\psi_J \rightarrow \psi'_{J'}$ transition. Because the reduced matrix elements are independent of the host, in our calculations were used the reduced matrix elements reported in [54].

The electric dipole line strength (S_{ED}) depends on the host, since the J–O parameters depend on the host. The magnetic dipole line strength (S_{MD}) is independent of the host.

Therefore, the magnetic dipole oscillator strength can be written as follow: $f_{MD} = n \times f_{MD}'$, where f_{MD}' is the magnetic dipole vacuum oscillator strength. The f_{MD}' values for magnetic dipole transitions of the Sm³⁺ ions were given in [58]. Magnetic dipole oscillator strengths for following ⁶H_{5/2} → ⁶F_{3/2}, ⁶F_{5/2}, ⁴G_{5/2}, ⁴F_{3/2} transitions were used for calculations of total oscillator strengths (f_{cal}). Thus, the formula (9) can be rewritten as:

$$f_{\text{cal}} = \frac{8\pi^2 m c \nu}{3h(2J+1)} \frac{(n^2+2)^2}{9n} \sum_{\lambda=2,4,6} \Omega_{\lambda} \left| \langle \psi_J \| U^{\lambda} \| \psi'_{J'} \rangle \right|^2 + n f_{MD}' \quad (12)$$

Table 1. The observed band positions (ν), experimental (f_{exp}) and calculated (f_{cal}) oscillator strengths as well as the root mean square deviation (σ_{rms}) for Sm³⁺ ions in glasses with Li₂B₄O₇:Sm, CaB₄O₇:Sm, and LiCaBO₃:Sm compositions containing 1.0 mol. % Sm₂O₃.

Transitions from ground level, ⁶ H _{5/2} ?	Li ₂ B ₄ O ₇ :Sm (1.0 mol. %)			CaB ₄ O ₇ :Sm (1.0 mol. %)			LiCaBO ₃ :Sm (1.0 mol. %)			Sm ³⁺ aqua-ion [54]
	ν (cm ⁻¹)	f_{exp} (×10 ⁻⁶)	f_{cal} (×10 ⁻⁶)	ν (cm ⁻¹)	f_{exp} (×10 ⁻⁶)	f_{cal} (×10 ⁻⁶)	ν (cm ⁻¹)	f_{exp} (×10 ⁻⁶)	f_{cal} (×10 ⁻⁶)	ν (cm ⁻¹)
⁶ F _{1/2}	6311	0.85	0.87	6310	0.45	0.45	6308	0.81	0.95	
⁶ F _{3/2}	6814	2.56	1.85	6831	2.24	1.68	6796	2.18	2.08	6630
⁶ F _{5/2}	7315	2.69	2.75	7334	2.64	3.03	7301	3.18	3.14	7100
⁶ F _{7/2}	8167	2.99	2.99	8189	4.15	4.15	8162	4.73	4.73	8000
⁶ F _{9/2}	9297	2.51	1.62	9308	2.96	2.52	9297	3.25	3.04	9200
⁴ F _{11/2}	10648	0.38	0.25	10600	0.43	0.40	10602	0.39	0.49	10500
⁴ G _{5/2}	17779	0.02	0.02	17802	0.02	0.02	17786	0.01	0.02	17900
⁴ F _{3/2}				19075	0.01	0.01	18966	0.02	0.01	18900
⁴ I _{9/2}	20503	0.16	0.06	20584	0.23	0.05	20583	0.21	0.08	
⁴ M _{15/2}	20991	0.74	0.28	20949	0.34	0.46	20999	0.67	0.56	20800
⁴ I _{11/2}	21370	0.36	0.10	21281	0.67	0.16	21327	0.64	0.20	21100
⁴ I _{13/2}	21700	0.22	0.30	21715	0.21	0.44	21680	0.30	0.52	21600
⁴ M _{17/2}	23703	0.09	0.06	23691	0.07	0.08	23633	0.07	0.09	
⁶ P _{3/2}	24860	5.19	5.19	24860	5.90	5.90	24799	5.94	5.94	24950
⁶ P _{7/2}	26685	0.63	0.93	26738	0.50	0.98				26750
⁴ D _{3/2}	27740	0.46	0.87							27700
σ_{rms} (×10 ⁻⁷)	$\sigma_{\text{rms}} = 3.53$			$\sigma_{\text{rms}} = 2.90$			$\sigma_{\text{rms}} = 1.61$			

where f_{ED} and f_{MD} are the electric and magnetic dipole contributions, h is the constant of Planck, J is the total angular momentum of the ground state, n is the refractive index, $(n^2+2)^2/9n$ is the local field correction for electric dipole transitions, n is the local field correction for magnetic dipole transitions, S_{ED} and S_{MD} are the electric and magnetic dipole line strengths, which are calculated using the following formulas [57]:

The intensity parameters were evaluated with usage Eq. (7) and Eq. (12) as well as least-square fitting procedure [59]. The fit accuracy between the experimental and calculated spectral intensities is given by root mean square (rms) deviation:

$$\sigma_{rms} = \sqrt{\frac{\sum (f_{exp} - f_{cal})^2}{N}} \quad (13)$$

where, N is the number of levels included in the fitting procedure. The obtained by us small rms deviation indicates good coincidence between the experimental and theoretical spectral intensities (see **Table 1**).

Intensity parameters (Ω_2 , Ω_4 , Ω_6) for $\text{Li}_2\text{B}_4\text{O}_7:\text{Sm}$, $\text{CaB}_4\text{O}_7:\text{Sm}$, and $\text{LiCaBO}_3:\text{Sm}$ glasses containing 1.0 mol. % Sm_2O_3 are presented in **Table 2**, where for comparison are presented the Sm^{3+} intensity parameters for other borate glasses. One can notice that the Ω_2 parameter is similar for $\text{LiCaBO}_3:\text{Sm}^{3+}$ and $\text{Li}_2\text{B}_4\text{O}_7:\text{Sm}^{3+}$ glasses, whereas the Ω_6 value is similar for $\text{LiCaBO}_3:\text{Sm}^{3+}$ and $\text{CaB}_4\text{O}_7:\text{Sm}^{3+}$ glasses.

The Ω_2 parameter is sensitive to the local structure of the RE^{3+} ions in crystal lattice or in glass network and strongly depends on the covalency of bond between RE^{3+} ions and ligand anions. The Ω_4 and Ω_6 parameters are related to the host matrix properties such as rigidity and

Ω_2 parameters reported for other borate glasses, in particular, for lithium zinc [39], bismuth [42], and zinc bismuth [43] borate glasses. The obtained Ω_2 values for investigated glasses are lower than the reported for lithium fluoroborate [36], sodium fluoroborate [32,41], and lithium calcium barium borate [38] glasses that allows to suggest that the symmetry of local environment for Sm^{3+} ions in our glasses is higher than that for these reported glasses.

For characterisation the optical quality of material often has been used the spectroscopic quality factor ($\chi = \Omega_4/\Omega_6$). For all investigated borate glasses the χ values are greater than unity ($\chi = 2.84$ for $\text{Li}_2\text{B}_4\text{O}_7:\text{Sm}$, $\chi = 1.99$ for $\text{CaB}_4\text{O}_7:\text{Sm}$, and $\chi = 1.64$ for $\text{LiCaBO}_3:\text{Sm}$), which indicate that these glasses are sufficiently stable and rigid. Generally, the stability and rigidity as well as spectroscopic quality factor of material decrease with increasing of amount of the heavy oxides in a glass composition. The obtained by us highest χ value (2.84) for $\text{Li}_2\text{B}_4\text{O}_7:\text{Sm}$ glass is larger than the χ values for other Sm-doped borate glasses with different basic

Table 2. Comparison of the intensity parameters ($\Omega_\lambda \times 10^{-20} \text{ cm}^2$) for Sm^{3+} centres in the Sm-doped borate glasses with different basic compositions.

Basic glass composition	Ω_2	Ω_4	Ω_6	Reference
$\text{Li}_2\text{B}_4\text{O}_7$ (or 33.33 Li_2O –66.66 B_2O_3)	3.19	5.68	2.00	[47] our data
CaB_4O_7 (or 33.33 CaO –66.66 B_2O_3)	1.66	6.34	3.19	[47] our data
LiCaBO_3 (or 25 Li_2O –50 CaO –25 B_2O_3)	3.81	6.20	3.79	[47] our data
Borate	6.36	6.02	3.51	[34]
30 Bi_2O_3 –70 B_2O_3	3.639	5.66	4.468	[42]
20 Li_2O –10 CaO –68 H_3BO_3	0.975	5.044	4.73	[37]
10 Li_2O –20 PbO –68 H_3BO_3	0.845	3.513	3.540	[37]
20 Li_2O –10 CaO –70 H_3BO_3	4.77	10.79	6.22	[38]
10 Li_2O –10 CaO –10 BaO –70 H_3BO_3	15.45	9.23	14.1	[38]
29.50 Li_2CO_3 –69.5 H_3BO_3	6.81	10.16	6.93	[36]
24.75 Li_2CO_3 –49.5 H_3BO_3 –24.75 LiF	5.56	9.21	5.50	[36]
20 ZnO –15 Bi_2O_3 –64 B_2O_3	1.93	1.87	1.79	[43]
49 B_2O_3 –25 Li_2O –25 NaF	3.92	8.17	5.82	[41]
49 B_2O_3 –25 CaO –25 NaF	4.18	8.30	6.38	[41]
25 Li_2CO_3 –64 H_3BO_3 –10 ZnF_2	1.73	9.47	8.93	[39]
53.33 PbO –13.33 PbF_2 –33.33 B_2O_3	3.41	2.92	2.17	[40]
8 Li_2O –7 BaO –15 La_2O_3 –70 B_2O_3	6.81	4.43	2.58	[35]
49 B_2O_3 –20 Bi_2O_3 –15 Li_2O –10 SrO –5 SrF_2	2.77	5.28	5.74	[33]

viscosity [60]. Large parameter Ω_2 indicates high covalency of the Sm – O bond and significant asymmetry of the oxygen polyhedra, which coordinated the Sm^{3+} ions. The value of Ω_2 parameter for $\text{Li}_2\text{B}_4\text{O}_7:\text{Sm}$ glass ($\Omega_2 = 3.19 \times 10^{-20} \text{ cm}^2$) is larger than that for $\text{CaB}_4\text{O}_7:\text{Sm}$ glass ($\Omega_2 = 1.66 \times 10^{-20} \text{ cm}^2$) due to more asymmetric local environment for Sm^{3+} ions in the $\text{Li}_2\text{B}_4\text{O}_7:\text{Sm}$ glass caused by differences in compensation of the excess charge by cationic vacancies at the following heterovalence substitutions: $\text{Sm}^{3+} \rightarrow \text{Li}^+$ (for $\text{Li}_2\text{B}_4\text{O}_7:\text{Sm}$ glass) and $\text{Sm}^{3+} \rightarrow \text{Ca}^{2+}$ (for $\text{CaB}_4\text{O}_7:\text{Sm}$ glass). The larger Ω_2 value ($\Omega_2 = 3.81 \times 10^{-20} \text{ cm}^2$), obtained for the mixed LiCaBO_3 alkali/alkaline glass, shows significant asymmetry of the oxygen polyhedra, which coordinated Sm^{3+} ions in this glass.

As we can see from **Table 2**, the values of Ω_2 parameter in the investigated glasses are comparable with

compositions reported in [32,33,36-44].

Photoluminescence spectra and radiative parameters of the Sm-doped borate glasses

The luminescence emission spectra of glasses with $\text{Li}_2\text{B}_4\text{O}_7:\text{Sm}$, $\text{LiKB}_4\text{O}_7:\text{Sm}$, $\text{CaB}_4\text{O}_7:\text{Sm}$, and $\text{LiCaBO}_3:\text{Sm}$ compositions containing 0.5 and 1.0 mol. % Sm_2O_3 registered at same experimental set-up ($\lambda_{\text{ex}} = 402 \text{ nm}$, $T = 300 \text{ K}$) are presented in **Fig. 4a**. The emission spectra consist of three intense and one weak emission bands in the 550 ÷ 750 nm spectral range. According to the Dieke energy level diagram for RE ions and referenced data [54, 55], the observed emission bands belong to following $f-f$ transitions of the Sm^{3+} ions: ${}^4\text{G}_{5/2} \rightarrow {}^6\text{H}_j$ ($J = 5/2 \div 11/2$), which are denoted in **Fig. 4a**.

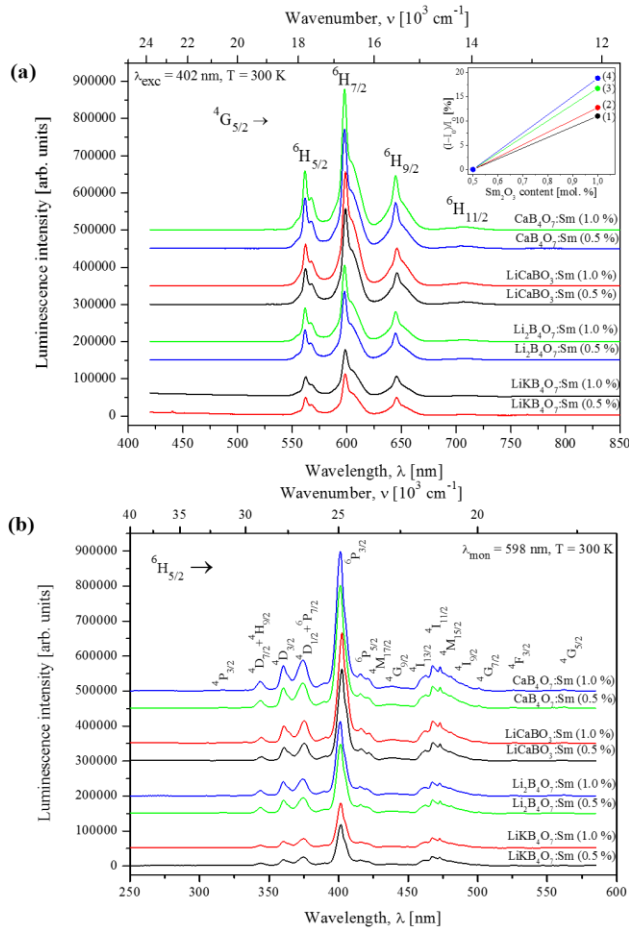


Fig. 4. The luminescence emission (a) and excitation (b) spectra of Sm^{3+} centres in the $\text{CaB}_4\text{O}_7:\text{Sm}$, $\text{LiCaBO}_3:\text{Sm}$, $\text{Li}_2\text{B}_4\text{O}_7:\text{Sm}$, and $\text{LiKB}_4\text{O}_7:\text{Sm}$ glasses (Sm_2O_3 content – 0.5 and 1.0 mol. %), recorded at $T = 300\text{ K}$. The increasing of relative emission intensity with increasing Sm_2O_3 content from 0.5 to 1.0 mol. % for glasses with $\text{Li}_2\text{B}_4\text{O}_7:\text{Sm}$ (1), $\text{LiKB}_4\text{O}_7:\text{Sm}$ (2), $\text{CaB}_4\text{O}_7:\text{Sm}$ (3), and $\text{LiCaBO}_3:\text{Sm}$ (4) compositions is shown in the inset of Fig. 4a.

The observed different intensities of the Sm^{3+} emission bands is caused by influence of the basic glass composition and Sm impurity concentration. One can notice that the emission intensity for alkaline earth borate glasses ($\text{CaB}_4\text{O}_7:\text{Sm}$ and $\text{LiCaBO}_3:\text{Sm}$) is more than two times higher than that for alkali borate glasses ($\text{Li}_2\text{B}_4\text{O}_7:\text{Sm}$ and $\text{LiKB}_4\text{O}_7:\text{Sm}$). With increasing the Sm_2O_3 content from 0.5 to 1.0 mol. % the relative integral intensity ($(I - I_0) / I_0$, where I and I_0 are integral intensities of the emission band corresponding ${}^4\text{G}_{5/2} \rightarrow {}^6\text{H}_{7/2}$ transition for samples containing 0.5 and 1.0 mol. % Sm_2O_3) approximately increases on 10, 12, 16, and 19 % for glasses with $\text{Li}_2\text{B}_4\text{O}_7:\text{Sm}$, $\text{LiKB}_4\text{O}_7:\text{Sm}$, $\text{CaB}_4\text{O}_7:\text{Sm}$, and $\text{LiCaBO}_3:\text{Sm}$ compositions, respectively (inset in **Fig. 4a**). This effect is related to considerable number of the $\text{Sm}^{3+} - \text{Sm}^{3+}$ pair centres in the investigated glasses containing 1.0 mol. % Sm_2O_3 that also reveals in their EPR spectra (see **Fig. 2**). Based on the presented results one can state that the optimal content of the Sm_2O_3 in glasses with $\text{Li}_2\text{B}_4\text{O}_7:\text{Sm}$, $\text{LiKB}_4\text{O}_7:\text{Sm}$, $\text{CaB}_4\text{O}_7:\text{Sm}$, and $\text{LiCaBO}_3:\text{Sm}$ compositions is about 1.0 mol. %.

In **Fig. 4b** are presented the Sm^{3+} luminescence excitation spectra in the $\text{Li}_2\text{B}_4\text{O}_7:\text{Sm}$, $\text{LiKB}_4\text{O}_7:\text{Sm}$,

$\text{CaB}_4\text{O}_7:\text{Sm}$, and $\text{LiCaBO}_3:\text{Sm}$ glasses containing 0.5 and 1.0 mol. % Sm_2O_3 , which were recorded at the same experimental conditions ($\lambda_{\text{mon}} = 598\text{ nm}$, $T = 300\text{ K}$). The influence of basic glass composition and Sm impurity concentration on the Sm^{3+} luminescence properties causes different intensities of their excitation bands like for emission bands that was discussed above. All observed luminescence excitation bands were assigned to the appropriate $f-f$ transitions of the Sm^{3+} ions in accordance with their energy level diagram and referenced data [54, 55]. The excitation spectra show that photoluminescence of Sm-doped borate glasses can be efficiently excite using near UV and violet – visible light. Most intense luminescence excitation band at 402 nm belongs to the ${}^6\text{H}_{5/2} \rightarrow {}^6\text{P}_{3/2}$ transition. The weak resolution of some Sm^{3+} excitation bands is connected with inhomogeneous broadening [61], caused by disordering of the glass structure that leads to slight differences in the local environments and crystal field parameters for Sm^{3+} centres in the glass network.

Thus, the luminescence (emission and excitation) spectra clearly prove that the Sm impurity are incorporated into the network of $\text{Li}_2\text{B}_4\text{O}_7$, LiKB_4O_7 , CaB_4O_7 , and LiCaBO_3 glasses as Sm^{3+} ions, exclusively. This result well agrees with published data for other Sm-doped borate glasses of different compositions [29, 35, 36, 40], which also demonstrate presence in glass network the Sm^{3+} ions, exclusively.

Obtained J–O intensity parameters Ω_λ ($\lambda = 2, 4, 6$) were used for calculations radiative parameters of the investigated glasses such as probabilities of the emission transitions, luminescence lifetimes, branching ratios, and emission cross-sections [59]. According to [59], the spontaneous emission rates from an excited state $\psi'J'$ to the final state ψJ (or probabilities of the radiative transitions, A_{rad}) can be calculated with usage the relation:

$$A_{rad}(\psi'J', \psi J) = A_{ED} + A_{MD} = \frac{64\pi^4 V^3}{3h(2J+1)} \left(\frac{n(n^2+2)^2}{9} S_{ED} + n^3 S_{MD} \right) \quad (14)$$

where, A_{MD} and A_{ED} are the magnetic and electric dipole contributions, n^3 and $n(n^2+2)^2/9$ are the local field corrections for the magnetic and electric dipole emission transitions, S_{ED} and S_{MD} are strengths of the electric and magnetic dipole lines, which are given by formulas (10) and (11).

The magnetic dipole term can be represented as $A_{MD} = n^3 \times A_{MD}'$, where A_{MD}' is the rates of the magnetic dipole vacuum spontaneous emission. The A_{MD}' values for the Sm^{3+} magnetic dipole transitions are given in [58]. Thus, the relation (14) can be rewritten as:

$$A_{rad}(\psi'J', \psi J) = \frac{64\pi^4 e^2 v^3}{3h(2J+1)} \frac{n(n^2+2)^2}{9} \sum_{\lambda=2,4,6} \Omega_\lambda \langle \psi'J' || U^\lambda || \psi J \rangle^2 + n^3 A_{MD}' \quad (15)$$

In particular, formula (15) was used for calculation the A_{rad} value for emission transitions ${}^4\text{G}_{5/2} \rightarrow {}^6\text{H}_{5/2}$, ${}^6\text{H}_{7/2}$ of the Sm^{3+} centres (see **Table 3**), because these transitions belong to mixed and contain the electric dipole and magnetic dipole contributions.

The total probabilities of radiative transitions (A_T) for an excited state $\psi'J'$ were obtained by summation of the $A_{rad}(\psi'J',\psi J)$ values for all emission transitions to the ψJ final states [59] according to relation:

$$A_T(\psi'J') = \sum_{\psi J} A_{rad}(\psi'J',\psi J) \quad (16)$$

The values of A_{rad} and A_T were used for calculation the branching ratio (β_{rad}) that is given by formula:

$$\beta_{rad}(\psi'J',\psi J) = \frac{A_{rad}(\psi'J',\psi J)}{A_T(\psi'J')} \quad (17)$$

The stimulated emission cross-section, $\sigma_e(\psi'J',\psi J)$, was calculated using the following relation:

$$\sigma_e(\psi'J',\psi J) = \frac{\lambda_p^4}{8\pi c n^2 \Delta\lambda_p} A_{rad}(\psi'J',\psi J) \quad (18)$$

where λ_p is the emission peak wavelength taken at

generation [62]. Thus, the calculated β values in the investigated glasses (see **Table 3**) show that the emission band at 598 nm corresponding to the ${}^4G_{5/2} \rightarrow {}^6H_{7/2}$ transition of the Sm^{3+} ions can be used for efficient laser generation in the visible region.

The cross-section of stimulated emission (σ_e) is very important parameter for evaluation of the efficiency of emission energy of the laser material. Highest emission cross-section ($\sigma_e = 8.09 \times 10^{-22} \text{ cm}^2$) is obtained for ${}^4G_{5/2} \rightarrow {}^6H_{7/2}$ transition in the $CaB_4O_7:Sm$ glass containing 1.0 mol. % Sm_2O_3 . The σ_e value for $CaB_4O_7:Sm$ glass (Sm_2O_3 content – 1.0 mol. %) is slightly lower than the σ_e value for Sm^{3+} centres in lithium calcium barium [38], lithium zinc [39], and zinc bismuth [43] borate glasses, comparable with the σ_e values for Sm^{3+} -doped lithium calcium borate [37], lithium strontium bismuth borate [33], sodium fluoroborate [41] glasses and larger than that the σ_e values for Sm^{3+} -doped lithium fluoroborate [36], sodium fluoroborate [32], lead borate [37], lead fluoroborate [40], zinc alumina bismuth borate [44] glasses.

Table 3. The emission peak positions (λ_p), effective linewidths ($\Delta\lambda_p$), probabilities of the radiative transitions (A_{rad}), which include the electric dipole (A_{ED}) and magnetic dipole (A_{MD}) contributions, experimental (β_{exp}) and calculated (β_{rad}) branching ratios, and stimulated emission cross-sections (σ_e) for emission transitions ${}^4G_{5/2} \rightarrow {}^6H_J$ ($J = 5/2, 7/2, 9/2, 11/2$) of the Sm^{3+} centres in the glasses with $Li_2B_4O_7:Sm$, $CaB_4O_7:Sm$, and $LiCaBO_3:Sm$ compositions containing 1.0 mol. % Sm_2O_3 .

Basic glass composition	Transition	λ_p (nm)	$\Delta\lambda_p$ (nm)	A_{ED} (s^{-1})	A_{MD} (s^{-1})	A_{rad} (s^{-1})	β_{exp}	β_{rad}	σ_e ($\times 10^{-22} \text{ cm}^2$)
$Li_2B_4O_7$	${}^4G_{5/2} \rightarrow {}^6H_{5/2}$	562	10.6	8.31	13.42	21.73	0.18	0.08	1.14
	${}^4G_{5/2} \rightarrow {}^6H_{7/2}$	598	13.7	105.36	11.11	116.47	0.54	0.43	6.05
	${}^4G_{5/2} \rightarrow {}^6H_{9/2}$	645	16.2	98.55		98.55	0.25	0.37	5.86
	${}^4G_{5/2} \rightarrow {}^6H_{11/2}$	704	29.2	33.07		33.07	0.03	0.12	1.55
CaB_4O_7	${}^4G_{5/2} \rightarrow {}^6H_{5/2}$	562	10.4	8.55	13.95	22.50	0.17	0.08	1.24
	${}^4G_{5/2} \rightarrow {}^6H_{7/2}$	598	13.6	137.01	11.56	148.57	0.55	0.50	8.09
	${}^4G_{5/2} \rightarrow {}^6H_{9/2}$	645	16.0	88.74		88.74	0.25	0.29	5.34
	${}^4G_{5/2} \rightarrow {}^6H_{11/2}$	704	29.0	40.74		40.74	0.03	0.13	1.92
$LiCaBO_3$	${}^4G_{5/2} \rightarrow {}^6H_{5/2}$	563	11.4	9.52	13.52	23.04	0.17	0.07	1.12
	${}^4G_{5/2} \rightarrow {}^6H_{7/2}$	599	14.0	145.82	11.20	157.02	0.56	0.47	7.98
	${}^4G_{5/2} \rightarrow {}^6H_{9/2}$	646	17.6	115.73		115.73	0.24	0.34	6.33
	${}^4G_{5/2} \rightarrow {}^6H_{11/2}$	706	28.2	41.74		41.74	0.03	0.12	2.02

maximum intensity and $\Delta\lambda_p = \frac{\int I(\lambda)d\lambda}{I_{max}}$ is the effective

linewidth. Positions of the emission peaks (λ_p), effective linewidths ($\Delta\lambda_p$), probabilities of the radiative transitions (A_{rad}), experimental (β_{exp}) and calculated (β_{rad}) branching ratios, and stimulated emission cross-section (σ_e) obtained for emission transitions ${}^4G_{5/2} \rightarrow {}^6H_J$ ($J = 5/2, 7/2, 9/2, 11/2$) in the glasses with $Li_2B_4O_7:Sm$, $CaB_4O_7:Sm$, and $LiCaBO_3:Sm$ compositions containing 1.0 mol. % Sm_2O_3 are presented in **Table 3**. It should be noted that all calculated radiative parameters depend on the basic glass composition (see **Table 3**).

The values of branching ratio (β) are used for characterisation of distribution of the emission transitions in the luminescence spectra. The β value higher than 0.5 for specific emission transition indicates that the most part of emission energy corresponds to this transition that potentially can be used for obtaining of the laser

The luminescence kinetics of Sm^{3+} centres

The luminescence decay curves for Sm^{3+} centres in the glasses with $Li_2B_4O_7:Sm$, $LiKB_4O_7:Sm$, $CaB_4O_7:Sm$, and $LiCaBO_3:Sm$ compositions, obtained for most intense orange-red emission band (${}^4G_{5/2} \rightarrow {}^6H_{7/2}$ transition) at the same experimental set-up ($\lambda_{exc} = 402 \text{ nm}$, $\lambda_{mon} = 598 \text{ nm}$, $T = 300 \text{ K}$) are presented in **Fig. 5a** using a semi-logarithmic scale. All obtained decay curves can be satisfactory described in the framework of single exponential approximation with lifetime values (τ_{exp}), which are presented in **Fig. 5a**.

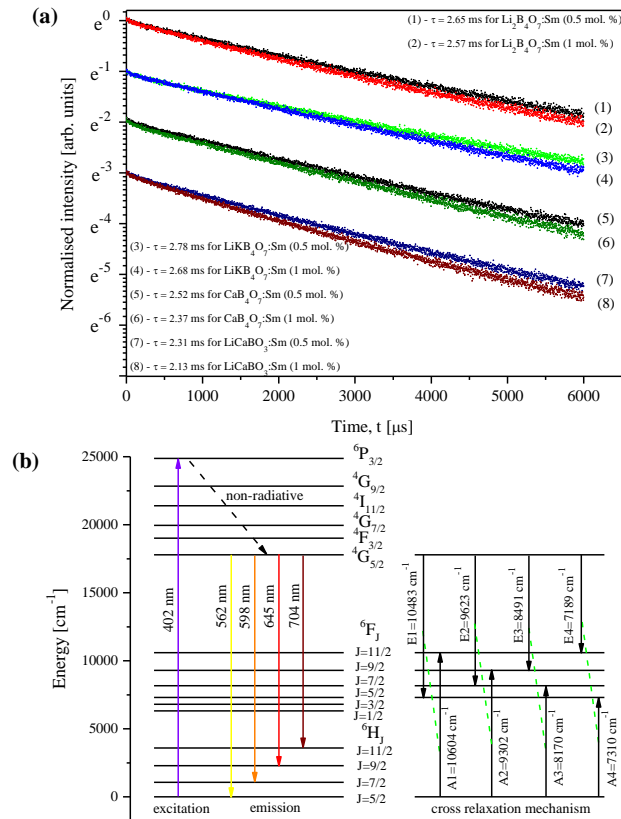


Fig. 5. (a) Luminescence decay curves for Sm^{3+} centres (${}^4\text{G}_{5/2} \rightarrow {}^6\text{H}_{7/2}$ transition, $\lambda_{\text{mon}} = 598 \text{ nm}$) in the $\text{Li}_2\text{B}_4\text{O}_7:\text{Sm}$, $\text{LiKB}_4\text{O}_7:\text{Sm}$, $\text{CaB}_4\text{O}_7:\text{Sm}$, and $\text{LiCaBO}_3:\text{Sm}$ glasses with 0.5 (curves 1, 3, 5, and 7) and 1.0 (curves 2, 4, 6, and 8) mol. % Sm_2O_3 , registered at $T = 300 \text{ K}$ under excitation with $\lambda_{\text{exc}} = 402 \text{ nm}$ (${}^6\text{H}_{5/2} \rightarrow {}^6\text{P}_{3/2}$ transition); (b) Diagram of the partial energy levels for Sm^{3+} centres in the $\text{Li}_2\text{B}_4\text{O}_7:\text{Sm}$ glass that shows also channels of excitation, emission and cross relaxation.

Table 4. Experimental (τ_{exp}) and radiative (τ_{rad}) lifetimes, cross-relaxation rates (W_{CR}), and quantum efficiencies (η) for the ${}^4\text{G}_{5/2}$ level of Sm^{3+} centres in the Sm-doped glasses with $\text{Li}_2\text{B}_4\text{O}_7$, CaB_4O_7 , and LiCaBO_3 basic compositions.

Glass composition	Sm_2O_3 content (mol. %)	τ_{exp} (ms)	τ_{rad} (ms)	W_{CR} (s^{-1})	η (%)
$\text{Li}_2\text{B}_4\text{O}_7:\text{Sm}$	0.5	2.65 ± 0.02	3.32	76	80
	1.0	2.57 ± 0.02		88	77
$\text{CaB}_4\text{O}_7:\text{Sm}$	0.5	2.52 ± 0.02	3.03	67	83
	1.0	2.37 ± 0.02		92	78
$\text{LiCaBO}_3:\text{Sm}$	0.5	2.31 ± 0.02	2.67	58	86
	1.0	2.13 ± 0.02		95	79

The obtained results show that the luminescence lifetimes strongly depend on the basic glass composition, local structure, and concentration of the impurity Sm^{3+} ions. Various lifetime values for identical amount of the Sm_2O_3 in the borate glasses with different compositions are caused by some differences in local environments of the Sm^{3+} centres in the glass network. Dependence of lifetime on the Sm^{3+} local structure in the $\text{Li}_2\text{B}_4\text{O}_7$, LiKB_4O_7 , CaB_4O_7 , and LiCaBO_3 glasses in detail was considered and discussed in [8].

In general case, the experimental lifetime (τ_{exp}) of an excited state can be defined by relation [63]:

$$\frac{1}{\tau_{\text{exp}}} = \frac{1}{\tau_{\text{rad}}} + W_{\text{MPR}} + W_{\text{CR}} \quad (19)$$

where τ_{rad} is the radiative lifetime, W_{MPR} and W_{CR} are rates of multiphonon relaxation and cross-relaxation. The W_{MPR} for our borate glasses is very small due to large energetic gap between the ${}^4\text{G}_{5/2}$ level and next lower level of the Sm^{3+} ions that is greater than the phonon energies of borate glasses. Therefore, the resonance energy transfer through cross-relaxation processes between $\text{Sm}^{3+} - \text{Sm}^{3+}$ pair centres, which are coupled by electric multipolar interactions is responsible for lifetime quenching in the investigated glasses containing relatively high concentration of the Sm^{3+} ions.

EPR spectroscopy confirms presence of the Sm^{3+} isolated and $\text{Sm}^{3+} - \text{Sm}^{3+}$ pair centres in the investigated glasses (see Fig. 2). Decreasing of the experimental lifetimes for Sm^{3+} centres with increasing of the Sm concentration in the investigated glasses (Fig. 5a) shows good correlation with corresponding increasing of EPR signal of the $\text{Sm}^{3+} - \text{Sm}^{3+}$ pair centres (Fig. 2). The obtained results show inhomogeneous distribution of the Sm^{3+} impurity centres in the glass network that leads to clustering of the Sm^{3+} ions in the glass host. As a result, it is possible the transfer of energy between the nearest Sm^{3+} impurity centres through the cross-relaxation and resonance energetic channels.

The diagram of partial energy levels along with radiative emissions and non-radiative relaxation from the ${}^4\text{G}_{5/2}$ level to different lower levels is presented in Fig. 5b, where four different cross-relaxation channels are shown. For luminescence quenching in the investigated borate glasses are responsible the following cross-relaxation channels: ${}^4\text{G}_{5/2} \rightarrow {}^6\text{F}_{5/2} \leftrightarrow {}^6\text{H}_{5/2} \rightarrow {}^6\text{F}_{11/2}$ (10500 cm^{-1}), ${}^4\text{G}_{5/2} \rightarrow {}^6\text{F}_{7/2} \leftrightarrow {}^6\text{H}_{5/2} \rightarrow {}^6\text{F}_{9/2}$ (9500 cm^{-1}), ${}^4\text{G}_{5/2} \rightarrow {}^6\text{F}_{9/2} \leftrightarrow {}^6\text{H}_{5/2} \rightarrow {}^6\text{F}_{7/2}$ (8300 cm^{-1}) and ${}^4\text{G}_{5/2} \rightarrow {}^6\text{F}_{11/2} \leftrightarrow {}^6\text{H}_{5/2} \rightarrow {}^6\text{F}_{5/2}$ (7200 cm^{-1}).

Radiative lifetimes of the excited ($\psi'J'$) state have been calculated using relation given in [59]:

$$\tau_{\text{rad}}(\psi'J') = \frac{1}{A_T(\psi'J')} \quad (20)$$

where, $A_T(\psi'J')$ is the total probability of radiative transitions from an excited state ($\psi'J'$). The calculated radiative lifetime values (τ_{rad}) for the Sm^{3+} level ${}^4\text{G}_{5/2}$ are presented in Table 4 for glasses with the $\text{Li}_2\text{B}_4\text{O}_7:\text{Sm}$, $\text{CaB}_4\text{O}_7:\text{Sm}$, and $\text{LiCaBO}_3:\text{Sm}$ compositions containing 0.5 and 1.0 mol. % Sm_2O_3 .

Quantum efficiency and quantum yield of luminescence of the investigated glasses

The experimental lifetime values (τ_{exp}), evaluated from decay curves, are shorter than the radiative lifetimes (τ_{rad}), which have been calculated with usage the J-O theory and relation (20) (see **Table 4**). The ratio of the experimental lifetime to the calculated radiative lifetime is defined as quantum efficiency ($\eta = \tau_{exp}/\tau_{rad}$) of the corresponding level. Calculated values of quantum efficiency for glasses with $\text{Li}_2\text{B}_4\text{O}_7:\text{Sm}$, $\text{CaB}_4\text{O}_7:\text{Sm}$, and $\text{LiCaBO}_3:\text{Sm}$ compositions (Sm_2O_3 content – 0.5 and 1.0 mol. %) are presented in **Table 4**. Quantum efficiencies for all investigated glasses containing 0.5 mol. % Sm_2O_3 are higher than quantum efficiencies for glasses containing 1.0 mol. % Sm_2O_3 due to lower their non-radiative rates. The highest value of quantum efficiency ($\eta \approx 86\%$) was obtained for $\text{LiCaBO}_3:\text{Sm}$ glass containing 0.5 mol. % Sm_2O_3 . High quantum efficiencies (about 80 %), obtained for all investigated Sm-doped glasses clearly show that these glasses can be considered as a promising materials for lasers and other luminescent devices.

Table 5. Quantum yields (QY) of luminescence for Sm^{3+} centres in the investigated glasses and some other Sm-doped oxide glasses, obtained by different authors.

Glass composition	QY, %	References
$\text{Li}_2\text{B}_4\text{O}_7 (\text{Li}_2\text{O}-\text{B}_2\text{O}_3):\text{Sm}$ (0.5 mol. %)	21.1	this work
$\text{Li}_2\text{B}_4\text{O}_7 (\text{Li}_2\text{O}-\text{B}_2\text{O}_3):\text{Sm}$ (1.0 mol. %)	19.8	this work
$\text{CaB}_4\text{O}_7 (\text{CaO}-\text{B}_2\text{O}_3):\text{Sm}$ (0.5 mol. %)	13.8	this work
$\text{LiCaBO}_3 (\text{Li}_2\text{O}-\text{CaO}-\text{B}_2\text{O}_3):\text{Sm}$ (0.5 mol. %)	9.5	this work
$\text{Na}_2\text{O}-\text{ZnO}-\text{PbO}-\text{GeO}_2-\text{TeO}_2$	6.0	[64]
$\text{Li}_2\text{O}-\text{K}_2\text{O}-\text{BaO}-\text{Bi}_2\text{O}_3-\text{TeO}_2$	7.6	[65]
$\text{Li}_2\text{O}-\text{Y}_2\text{O}_3-\text{Al}_2\text{O}_3-\text{SiO}_2$	11.6	[66]
$\text{Li}_2\text{O}-\text{K}_2\text{O}-\text{ZnO}-\text{BaO}-\text{Sb}_2\text{O}_3-\text{B}_2\text{O}_3$	13.3	[67]

The quantum yield (QY) is used as a selection criterion for practical applications of luminescent materials. The QY is defined as ratio of photons emitted to photons absorbed. The measured quantum yields for our Sm-doped glasses are presented in **Table 5**. The highest values of quantum yields were obtained for $\text{Li}_2\text{B}_4\text{O}_7:\text{Sm}$ glasses containing 0.5 mol. % Sm_2O_3 (QY = 21.1 %) and 1.0 mol. % Sm_2O_3 (QY = 19.8 %). For $\text{CaB}_4\text{O}_7:\text{Sm}$ glass containing 0.5 mol. % Sm_2O_3 that show highest value of the stimulated emission cross-section (σ_e) for Sm^{3+} centres (${}^4\text{G}_{5/2} \rightarrow {}^6\text{H}_{7/2}$ transition) the corresponding quantum yield equals 13.83 %.

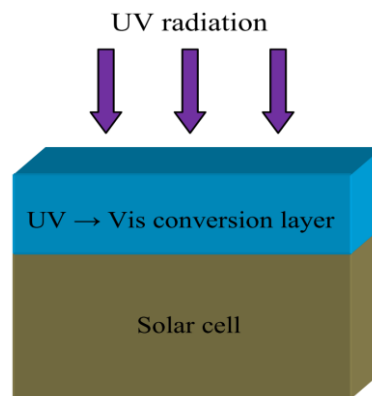
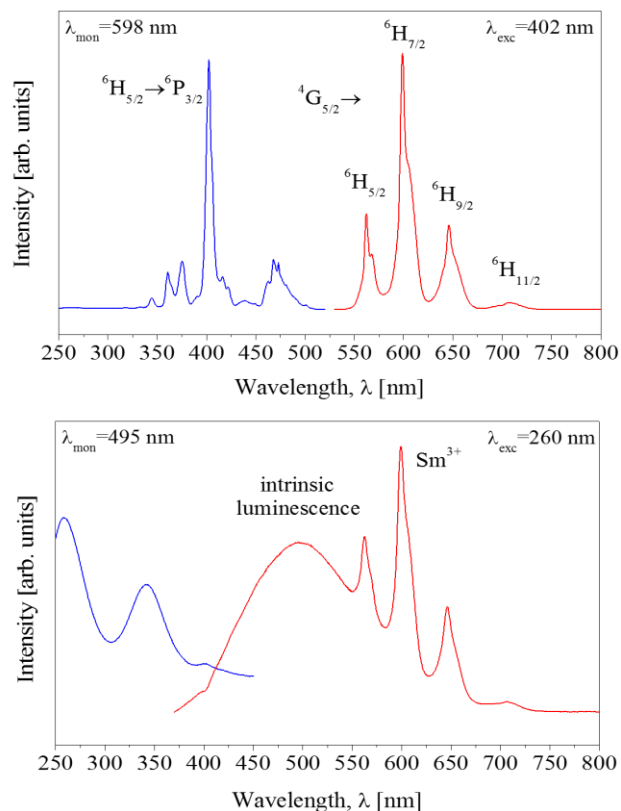


Fig. 6. The summarised luminescence excitation and emission spectra as well as schematic representation of the UV – visible down-conversion layer for Si solar cell, based on the Sm-doped borate glass.

The obtained quantum yields for $\text{Li}_2\text{B}_4\text{O}_7:\text{Sm}$ and $\text{CaB}_4\text{O}_7:\text{Sm}$ glasses are considerable larger than those in the Sm^{3+} -doped germanotellurite ($\text{Na}_2\text{O}-\text{ZnO}-\text{PbO}-\text{GeO}_2-\text{TeO}_2$) (QY = 6.0 %) [64], heavy metal tellurite ($\text{Li}_2\text{O}-\text{K}_2\text{O}-\text{BaO}-\text{Bi}_2\text{O}_3-\text{TeO}_2$) (QY = 7.55 %) [65], and lithium yttrium aluminum silicate ($\text{Li}_2\text{O}-\text{Y}_2\text{O}_3-\text{Al}_2\text{O}_3-\text{SiO}_2$) (QY = 11.58 %) [66] glasses and it is comparable with quantum yield of the Sm^{3+} -doped alkaline-earth borate ($\text{Li}_2\text{O}-\text{K}_2\text{O}-\text{ZnO}-\text{BaO}-\text{Sb}_2\text{O}_3-\text{B}_2\text{O}_3$) glass (QY = 13.29%) [67] (see **Table 5**).

Thus, relatively simple and inexpensive producing technology of the investigated Sm-doped borate glasses, their high transparency in the wide spectral range, dominant orange – red emission, large stimulated emission cross-section, high quantum efficiency and quantum yield of luminescence allow to consider these

borate glasses as perspective luminescent and laser materials in the visible spectral range. Based on experimental results we can state that the UV radiation that absorbed by Sm-doped borate glasses could be efficiently down-converted into the visible light. Hence, the investigated Sm-doped borate glasses can be successfully used as down-conversion (UV – visible) and protection layers in the Si solar cells (see Fig. 6), working in the regions with intense UV-radiation. The layer of the Sm-doped borate glass placed on the front side of solar cell could efficiently convert UV photons into visible light, where the Si-based solar cells exhibit a better spectral response and efficiency.

Conclusion

A series of Sm-doped glasses with $\text{Li}_2\text{B}_4\text{O}_7$, LiKB_4O_7 , CaB_4O_7 , and LiCaBO_3 compositions of high optical quality have been obtained and detailed investigated using EPR and optical spectroscopy techniques as well as Judd–Ofelt analysis. Basing on the obtained results it was shown the following:

- The Sm impurity is incorporated into the $\text{Li}_2\text{B}_4\text{O}_7$, LiKB_4O_7 , CaB_4O_7 , and LiCaBO_3 glass network exclusively as Sm^{3+} ($4f^5$, $^6\text{H}_{5/2}$) ions and forms the Sm^{3+} single and $\text{Sm}^{3+} - \text{Sm}^{3+}$ pair centres with characteristic EPR, optical absorption and photoluminescence spectra.
- The EPR and optical (absorption, emission and luminescence excitation) spectra as well as luminescence kinetics of the Sm^{3+} centres in the $\text{Li}_2\text{B}_4\text{O}_7:\text{Sm}$, $\text{LiKB}_4\text{O}_7:\text{Sm}$, $\text{LiCaBO}_3:\text{Sm}$, and $\text{CaB}_4\text{O}_7:\text{Sm}$ glasses were investigated studied and analysed in comparison with borate glasses of other compositions.
- Optical absorption spectra of the Sm^{3+} centres in $\text{Li}_2\text{B}_4\text{O}_7:\text{Sm}$, $\text{CaB}_4\text{O}_7:\text{Sm}$, and $\text{LiCaBO}_3:\text{Sm}$ glasses were analysed in the framework of Judd–Ofelt theory. Experimental and theoretical oscillator strengths as well as J–O intensity parameters have been calculated.
- Radiative parameters such as probabilities of transitions, branching ratios, stimulated emission cross-sections, and radiative lifetimes were evaluated for $^4\text{G}_{5/2} \rightarrow ^6\text{H}_J$ ($J = 5/2, 7/2, 9/2, \text{ and } 11/2$) emission transitions of the Sm^{3+} centres.
- The experimental emission decay curves for Sm^{3+} centres ($^4\text{G}_{5/2} \rightarrow ^6\text{H}_{7/2}$ transition) in all investigated glasses were satisfactory described in the framework of single exponent approximation. Obtained experimental lifetimes show typical values for Sm^{3+} centres and depend on the basic glass composition and Sm concentration. Quantum efficiencies have been calculated and quantum yields of luminescence have been measured for Sm^{3+} emission transitions in $\text{Li}_2\text{B}_4\text{O}_7:\text{Sm}$, $\text{CaB}_4\text{O}_7:\text{Sm}$, and $\text{LiCaBO}_3:\text{Sm}$ glasses.
- Appropriate optical and luminescence properties, high quantum efficiency ($\eta \approx 80\%$) and quantum yield ($\text{QY} = 14 - 20\%$) of the Sm^{3+} emission in $\text{Li}_2\text{B}_4\text{O}_7:\text{Sm}$, $\text{CaB}_4\text{O}_7:\text{Sm}$, and $\text{LiCaBO}_3:\text{Sm}$ glasses clearly show that these glasses represent very promising luminescent materials, especially for UV–visible photo-conversion

layers, which can be used in the Si solar cells working in the regions with intense UV-radiation including outer space.

Acknowledgements

The authors would like to thank Dr. A. Drzewiecki from Institute of Physics of the University of Zielona Góra (Poland) for registration of the EPR and luminescence spectra as well as decay curves and M.Sc. A. Watras from Institute of Low Temperature and Structure Research Polish Academy of Sciences (Wrocław, Poland) for quantum yield measurements.

References

1. Ehrst D.; *Glass Technol.*, **2000**, *41*, 182.
2. Yiannopoulos Y.D.; Chryssikos G.D.; Kamitsos E.I.; *Phys. Chem. Glasses*, **2001**, *42*, 164.
3. El-Adawy A.; Khaled N.E.; El-Sersy A.R.; Hussein A.; Donya H.; *Appl. Radiat. Isot.*, **2010**, *68*, 1132.
DOI: [10.1016/j.apradiso.2010.01.017](https://doi.org/10.1016/j.apradiso.2010.01.017)
4. Padyak B.V.; Mudry S.I.; Kulyk Y.O.; Drzewiecki A.; Adamiv V.T.; Burak Y.V.; Teslyuk I.M.; *Mater. Sci. Poland*, **2012**, *30*, 264.
DOI: [10.2478/s13536-012-0032-1](https://doi.org/10.2478/s13536-012-0032-1)
5. Padyak B.V.; Adamiv V.T.; Burak Ya.V.; Kolcun M.; *Phys. B*, **2013**, *412*, 79.
DOI: [10.1016/j.physb.2012.12.007](https://doi.org/10.1016/j.physb.2012.12.007)
6. Padyak B.; Drzewiecki A.; *J. Non-Cryst. Solids*, **2013**, *367*, 58.
DOI: [10.1016/j.jnoncrysol.2013.02.018](https://doi.org/10.1016/j.jnoncrysol.2013.02.018)
7. Padyak B.V.; Kindrat I.I.; Protsiuk V.O.; Drzewiecki A.; *Ukr. J. Phys. Opt.*, **2014**, *15*, 103.
DOI: [10.3116/16091833/15/3/103/2014](https://doi.org/10.3116/16091833/15/3/103/2014)
8. Kindrat I.I.; Padyak B.V.; Drzewiecki A.; *J. Lumin.*, **2015**, *166*, 264.
DOI: [10.1016/j.jlumin.2015.05.051](https://doi.org/10.1016/j.jlumin.2015.05.051)
9. Blasse G.; Grabmaier B.C.; *Luminescent materials*; Springer Verlag, Berlin, **1994**.
DOI: [10.1007/978-3-642-79017-1](https://doi.org/10.1007/978-3-642-79017-1)
10. Bünzli J.-C.; Piguat C.; *Chem. Soc. Rev.*, **2005**, *34*, 1048.
DOI: [10.1039/B406082M](https://doi.org/10.1039/B406082M)
11. Arun Kumar R.; *J. Chem.*, **2013**, 154862.
DOI: [10.1155/2013/154862](https://doi.org/10.1155/2013/154862)
12. Xue D.; Betzler K.; Hesse H.; Lammers D.; *Solid State Commun.*, **2000**, *114*, 21.
DOI: [10.1016/S0038-1098\(99\)00579-7](https://doi.org/10.1016/S0038-1098(99)00579-7)
13. Sasaki T.; Mori Y.; Yoshimura M.; Yap Y.K.; Kamimura T.; *Mater. Sci. Eng. R*, **2000**, *30*, 1.
DOI: [10.1016/S0927-796X\(00\)00025-5](https://doi.org/10.1016/S0927-796X(00)00025-5)
14. Adamiv V.T.; Burak Ya.V.; Teslyuk I.M.; *J. Cryst. Growth*, **2006**, *289*, 157.
DOI: [10.1016/j.jcrysgro.2005.11.013](https://doi.org/10.1016/j.jcrysgro.2005.11.013)
15. Mariselvam K.; Arun Kumar R.; *Univers. J. Chem.*, **2016**, *4*, 55.
DOI: [10.13189/ujc.2016.040202](https://doi.org/10.13189/ujc.2016.040202)
16. Prokic M.; *Radiat. Meas.*, **2001**, *33*, 393.
DOI: [10.1016/S1350-4487\(01\)00039-7](https://doi.org/10.1016/S1350-4487(01)00039-7)
17. Fernandes A.C.; Osvay M.; Santos J.P.; Holovey V.; Ignatovych M.; *Radiat. Meas.*, **2008**, *43*, 476.
DOI: [10.1016/j.radmeas.2008.01.004](https://doi.org/10.1016/j.radmeas.2008.01.004)
18. Un A.; Investigation of dopant effect on some TL dosimeters containing boron, *Radiat. Phys. Chem.*, **2013**, *85*, 23.
DOI: [10.1016/j.radphyschem.2012.10.016](https://doi.org/10.1016/j.radphyschem.2012.10.016)
19. Ishii M.; Kuwano Y.; Asaba S.; Asai T.; Kawamura M.; Senguttuvan N.; Hayashi T.; Koboyashi M.; Nikl M.; Hosoya S.; Sakai K.; Adachi T.; Oku T.; Shimizu H.M.; *Radiat. Meas.*, **2004**, *38*, 571.
DOI: [10.1016/j.radmeas.2004.03.017](https://doi.org/10.1016/j.radmeas.2004.03.017)
20. Zadneprowski B.I.; Eremin N.V.; Paskhalov A.A.; *Funct. Mater.*, **2005**, *12*, 261.
21. Deeg E.W.; Industrial Borate Glasses, In Borate glasses structure, properties; Pye L.D.; Frechette V.D.; Kreidl N.J. (Eds.); Plenum Press: New York, **1978**, pp. 587–596.
22. Komatsu R.; Kawano H.; Oumarou Z.; Shinoda K.; Petrov V.; *J. Cryst. Growth*, **2005**, *275*, 843.
DOI: [10.1016/j.jcrysgro.2004.11.122](https://doi.org/10.1016/j.jcrysgro.2004.11.122)

23. Burak Ya.V.; Kopko B.N.; Lysejko I.T.; Matkovskii A.O.; Slipetskii R.R.; Ulmanis U.A.; *Inorg. Mater.*, **1989**, 25, 1226.
24. Burak Ya.V.; Padlyak B.V.; Shevel V.M.; *Nucl. Instrum. Methods Phys. Res., Sect. B*, **2002**, 191, 633.
DOI: [10.1016/S0168-583X\(02\)00624-9](https://doi.org/10.1016/S0168-583X(02)00624-9)
25. Burak Ya.V.; Padlyak B.V.; Shevel V.M.; *Radiat. Eff. Defects Solids*, **2002**, 157, 1101.
DOI: [10.1080/10420150215791](https://doi.org/10.1080/10420150215791)
26. Judd B.R.; *Phys. Rev.*, **1962**, 127, 750.
DOI: [10.1103/PhysRev.127.750](https://doi.org/10.1103/PhysRev.127.750)
27. Ofelt G.S.; *J. Chem. Phys.*, **1962**, 37, 511.
DOI: [10.1063/1.1701366](https://doi.org/10.1063/1.1701366)
28. Yen W.M.; Shionoya Sh.; Yamamoto H. (Eds.); Phosphor handbook, CRC Press, **2006**.
29. Kaur P.; Kaur S.; Singh G.P.; Singh D.P.; *Solid State Commun.*, **2013**, 171, 22.
DOI: [10.1016/j.ssc.2013.07.021](https://doi.org/10.1016/j.ssc.2013.07.021)
30. Kaur P.; Kaur S.; Singh G.P.; Singh D.P.; *J. Alloys Compd.*, **2014**, 588, 394.
DOI: [10.1016/j.jallcom.2013.10.181](https://doi.org/10.1016/j.jallcom.2013.10.181)
31. Li P.; Wang Zh.; Yang Z.; Guo Q.; Li X.; *J. Lumin.*, **2010**, 130, 222.
DOI: [10.1016/j.jlumin.2009.08.010](https://doi.org/10.1016/j.jlumin.2009.08.010)
32. Umamaheswari D.; Jamalalah B.C.; Sasikala T.; Kim I.-G.; Moorthy L.R.; *J. Non-Cryst. Solids*, **2012**, 358, 782.
DOI: [10.1016/j.jnoncrysol.2011.12.023](https://doi.org/10.1016/j.jnoncrysol.2011.12.023)
33. Rajesh D.; Balakrishna A.; Ratnakaram Y.C.; *Opt. Mater.*, **2012**, 35, 108.
DOI: [10.1016/j.optmat.2012.07.011](https://doi.org/10.1016/j.optmat.2012.07.011)
34. Boehm L.; Reisfeld R.; Spector N.; *J. Solid State Chem.*, **1979**, 28, 75.
DOI: [10.1016/0022-4596\(79\)90060-4](https://doi.org/10.1016/0022-4596(79)90060-4)
35. Lin H.; Yang D.; Liu G.; Ma T.; Zhai B.; An Q.; Yu J.; Wang X.; Liu X.; Pun E.Y.-B.; *J. Lumin.*, **2005**, 113, 121.
DOI: [10.1016/j.jlumin.2004.09.115](https://doi.org/10.1016/j.jlumin.2004.09.115)
36. Jayasankar C.K.; Babu P.; *J. Alloys Compd.*, **2000**, 307, 82.
DOI: [10.1016/S0925-8388\(00\)00888-4](https://doi.org/10.1016/S0925-8388(00)00888-4)
37. Srivastava P.; Rai S.B.; Rai D.K.; *Spectrochim. Acta, Part A*, **2004**, 60, 637.
DOI: [10.1016/S1386-1425\(03\)00273-7](https://doi.org/10.1016/S1386-1425(03)00273-7)
38. Tripathi G.; Rai V.K.; Rai S.B.; *Appl. Phys. B*, **2006**, 84, 459.
DOI: [10.1007/s00340-006-2239-5](https://doi.org/10.1007/s00340-006-2239-5)
39. Thomas S.; Rasool S.N.; Rathaiah M.; Venkatramu V.; Joseph C.; Unnikrishnan N.V.; *J. Non-Cryst. Solids*, **2013**, 376, 106.
DOI: [10.1016/j.jnoncrysol.2013.05.022](https://doi.org/10.1016/j.jnoncrysol.2013.05.022)
40. Filho A.G.S.; Filho J.M.; Melo F.E.A.; Custódio M.C.C.; Lebullenger R.; Hernandez A.C.; *J. Phys. Chem. Solids*, **2000**, 61, 1535.
DOI: [10.1016/S0022-3697\(00\)00032-9](https://doi.org/10.1016/S0022-3697(00)00032-9)
41. Rayappan I.A.; Selvaraju K.; Marimuthu K.; *Phys. B*, **2011**, 406, 548.
DOI: [10.1016/j.physb.2010.11.037](https://doi.org/10.1016/j.physb.2010.11.037)
42. Saisudha M.B.; Ramakrishna J.; *Opt. Mater.*, **2002**, 18, 403.
DOI: [10.1016/S0925-3467\(01\)00181-1](https://doi.org/10.1016/S0925-3467(01)00181-1)
43. Agarwal A.; Pal I.; Sanghi S.; Aggarwal M.P.; *Opt. Mater.*, **2009**, 32, 339.
DOI: [10.1016/j.optmat.2009.08.012](https://doi.org/10.1016/j.optmat.2009.08.012)
44. Swapna K.; Mahamuda Sk.; Srinivasa Rao A.; Shakya S.; Sasikala T.; Haranath D.; Vijaya Prakash G.; *Spectrochim. Acta, Part A*, **2014**, 125, 53.
DOI: [10.1016/j.saa.2014.01.025](https://doi.org/10.1016/j.saa.2014.01.025)
45. Padlyak B.; Ryba-Romanowski W.; Lisiecki R.; Adamiv V.; Burak Y.; Teslyuk I.; Banaszak-Piechowska A.; *Opt. Appl.*, **2010**, 40, 427.
46. Kindrat I.I.; Padlyak B.V.; Drzewiecki A.; *J. Phys. Stud.*, **2014**, 18, 2998.
47. Kindrat I.I.; Padlyak B.V.; Lisiecki R.; *Opt. Mater.*, **2015**, 49, 241.
DOI: [10.1016/j.optmat.2015.09.024](https://doi.org/10.1016/j.optmat.2015.09.024)
48. Iton L.E.; Turkevich J.; *J. Phys. Chem.*, **1977**, 81, 435.
DOI: [10.1021/j100520a015](https://doi.org/10.1021/j100520a015)
49. Padlyak B.V.; Gutsze A.; *Appl. Magn. Reson.*, **1998**, 14, 59.
DOI: [10.1007/BF03162007](https://doi.org/10.1007/BF03162007)
50. Padlyak B.; Ryba-Romanowski W.; Lisiecki R.; Pieprzyk B.; Drzewiecki A.; Adamiv V.; Burak Y.; Teslyuk I.; *Opt. Appl.*, **2012**, 42, 365.
51. Griscom D.L.; *J. Non-Cryst. Solids*, **1980**, 40, 211.
DOI: [10.1016/0022-3093\(80\)90105-2](https://doi.org/10.1016/0022-3093(80)90105-2)
52. Brodbeck C.M.; *J. Non-Cryst. Solids*, **1980**, 40, 305.
DOI: [10.1016/0022-3093\(80\)90108-8](https://doi.org/10.1016/0022-3093(80)90108-8)
53. Brodbeck C.M.; Bukrey R.R.; *Phys. Rev. B*, **1981**, 24, 2334.
DOI: [10.1103/PhysRevB.24.2334](https://doi.org/10.1103/PhysRevB.24.2334)
54. Carnall W.T.; Fields P.R.; Rajnak K.; *J. Chem. Phys.*, **1968**, 49, 4424.
DOI: [10.1063/1.1669893](https://doi.org/10.1063/1.1669893)
55. Carnall W.T.; Beitz J.V.; Crosswhite H.; Rajnak K.; Mann J.B.; Spectroscopic properties of the f-elements in compounds and solution, In Systematic and the properties of the lanthanides; Sinha S.P. (Ed.); Reidel, Dordrecht, **1983**, pp. 389–450.
DOI: [10.1007/978-94-009-7175-2_9](https://doi.org/10.1007/978-94-009-7175-2_9)
56. Göllner-Walrand C.; Binnemans K.; Spectral intensities of f-f transitions, In Handbook on the Physics and Chemistry of Rare Earths; Gschneidner Jr K.A.; Eyring L. (Eds.); Elsevier B.V., **1998**, pp. 101–264.
DOI: [10.1016/S0168-1273\(98\)25006-9](https://doi.org/10.1016/S0168-1273(98)25006-9)
57. Gaft M.; Reisfeld R.; Panczer G.; Modern Luminescence Spectroscopy of Minerals and Materials, Springer Berlin Heidelberg, **2005**.
DOI: [10.1007/b137490](https://doi.org/10.1007/b137490)
58. Dodson C.M.; Zia R.; *Phys. Rev. B*, **2012**, 86, 125102.
DOI: [10.1103/PhysRevB.86.125102](https://doi.org/10.1103/PhysRevB.86.125102)
59. Walsh B.M.; Judd-Ofelt theory: principles and practices, In: Advances in Spectroscopy for Lasers and Sensing; Di Bartolo B.; Forte O. (Eds.); Springer, Dordrecht, **2006**, pp. 403–433.
DOI: [10.1007/1-4020-4789-4_21](https://doi.org/10.1007/1-4020-4789-4_21)
60. Jorgensen C.K.; Reisfeld R.; *J. Less-Common Met.*, **1983**, 93, 107.
DOI: [10.1016/0022-5088\(83\)90454-X](https://doi.org/10.1016/0022-5088(83)90454-X)
61. Vij D.R. (Ed.); Luminescence of Solids; Plenum Press: New York, **1998**.
DOI: [10.1007/978-1-4615-5361-8](https://doi.org/10.1007/978-1-4615-5361-8)
62. Dignonnet M.J.F. (Ed.); Rare-Earth-Doped Fiber Lasers and Amplifiers; CRC Press, **2001**.
63. Miyakawa T.; Dexter D.L.; *Phys. Rev. B*, **1970**, 1, 2961.
DOI: [10.1103/PhysRevB.1.2961](https://doi.org/10.1103/PhysRevB.1.2961)
64. Wang F.; Chen B.J.; Lin H.; Pun E.Y.B.; *J. Quant. Spectrosc. Radiat. Transfer*, **2014**, 147, 63.
DOI: [10.1016/j.jqsrt.2014.05.014](https://doi.org/10.1016/j.jqsrt.2014.05.014)
65. Lin H.; Wang X.Y.; Li C.M.; Li X.J.; Tanabe S.; Yu J.Y.; *Spectrochim. Acta, Part A*, **2007**, 67, 1417.
DOI: [10.1016/j.saa.2006.10.039](https://doi.org/10.1016/j.saa.2006.10.039)
66. Fu F.; Chen B.; Shen L.; Pun E.Y.B.; Lin H.; *J. Alloys Compd.*, **2014**, 582, 265.
DOI: [10.1016/j.jallcom.2013.08.040](https://doi.org/10.1016/j.jallcom.2013.08.040)
67. Shen L.F.; Chen B.J.; Pun E.Y.B.; Lin H.; *J. Lumin.*, **2015**, 160, 138.
DOI: [10.1016/j.jlumin.2014.11.052](https://doi.org/10.1016/j.jlumin.2014.11.052)

A Monthly Journal

Publish your article in this journal

Advanced Materials Letters is an official international journal of International Association of Advanced Materials (IAAM, www.iaamonline.org) published monthly by VBRI Press AB from Sweden. The journal is intended to provide high-quality peer-review articles in the fascinating field of materials science and technology particularly in the area of structure, synthesis and processing, characterisation, advanced-state properties and applications of materials. All published articles are indexed in various databases and are available download for free. The manuscript management system is completely electronic and has fast and fair peer-review process. The journal includes review article, research article, notes, letter to editor and short communications.

www.vbripress.com/aml

Copyright © 2017 VBRI Press AB, Sweden